Available online at www.sciencedirect.com

jmr&t Journal of Materials Research and Technology

journal homepage: www.elsevier.com/locate/jmrt

Original Article

C–O–H_2 ternary diagram for evaluation of carbon activity in CH_4-containing gas mixtures

T.R. Ribeiro [a,b,*], J.B. Ferreira Neto [a], C. Takano [b], J.G.R. Poço [c], L. Kolbeinsen [d], E. Ringdalen [e]

[a] Institute for Technological Research - IPT, Av. Prof Almeida Prado, 532, São Paulo, SP, 05508-901, Brazil
[b] Polytechnic School of the University of São Paulo. Dept. of Metallurgical and Materials Engineering, Av. Prof. Mello Moraes, 2463, São Paulo, SP, 05508-030, Brazil
[c] Centro Universitario FEI. Chemical Engineering Dept., Av. Humberto de Alencar Castelo Branco, 3972, São Bernardo do Campo, SP, 09850-901, Brazil
[d] Norwegian University of Science and Technology, Alfred Getz vei 2, Trondheim, 7034, Norway
[e] SINTEF Industry, Alfred Getz vei 2, Trondheim, 7034, Norway

ARTICLE INFO

Article history:
Received 10 February 2021
Accepted 19 May 2021
Available online 29 May 2021

Keywords:
Carbon activity
Thermodynamics
Direct reduction
Carburization
Methane
Methanol
Ethanol
Reforming
Ternary diagram

ABSTRACT

The C–O–H_2 ternary diagram is presented to characterize the carbon activity in equilibrium with gas mixtures containing CH_4, CO, CO_2, H_2O, and H_2 at different temperatures and pressures. The three reactions for carbon deposition from CH_4, CO, and CO + H_2 are considered jointly, and the combined equilibrium carbon activity is calculated. The lines on the diagram show a set of gas compositions that is in equilibrium with a defined value of carbon activity at a given temperature and pressure. It was possible to verify that carbon activity in equilibrium with the direct reduction process gas of Midrex is 0.15 and of Energiron ZR is 8.5, explaining the higher carbon content in the reduced iron for the latter. In the case of steam reforming of methane and methanol, carbon activity in usual industrial conditions are of 0.35 and 0.73 respectively. Finally steam reforming of ethanol was evaluated and it was shown that carbon deposition is expected at 240 °C but would be avoided at temperatures of 500 °C and higher in equilibrium conditions. The proposed diagram could be useful in many chemical, catalytic, and metallurgical processes for study or prevention of carbon formation.

1. Introduction

Carbon deposition is a theme of interest in chemical and metallurgical processes. It must be avoided in the Fischer–Tropsch synthesis and in the reforming of natural gas, hydrocarbons, and alcohols. In such processes, carbon deposition increases pressure drop in a catalytic bed, causes catalyst deactivation [1,2], and a corrosion failure named metal dusting [3–11]. Metal dusting is a catastrophic event

* Corresponding author.
E-mail addresses: tiago.ramos00@gmail.com, tiagorr@ipt.br (T.R. Ribeiro).
https://doi.org/10.1016/j.jmrt.2021.05.033

that disintegrates metals and alloys into fine particles composed of graphite and metallic material. The phenomenon typically occurs in the presence of reducing and highly carburizing atmospheres (carbon activity - $a_C > 1$) at temperatures normally higher than 400 °C. It leads to a reduced metal catalyst lifetime and damages structural materials. On the other hand, in the direct reduction of iron ore, carbon deposition into reduced iron ore pellets is desirable since it is a source of chemical energy in the subsequent steps of steel production [11–13,24].

The chemical reactions that cause carbon deposition are shown in Eqs. (1) through (3):

$$CO + H_2 = C + H_2O \ \Delta H^0 = -131.3 \text{ kJ/mol} \quad (1)$$

$$2\ CO = C + CO_2 \ \Delta H^0 = -172.5 \text{ kJ/mol} \quad (2)$$

$$CH_4 = C + 2H_2 \ \Delta H^0 = +74.9 \text{ kJ/mol} \quad (3)$$

Reactions 1 and 2 are the most important in the occurrence of metal dusting in reforming of hydrocarbons, since temperatures in such processes are lower than 900 °C [3–10]. Carburization of reduced iron may happen by all three reactions, depending on process parameters. Metallic iron is formed at temperatures above 700 °C in reducing conditions. CO plays an essential role as a carburizing agent up to 850 °C [12]. Modern practices of direct reduction processes include injection of natural gas in the high-temperature zone of the reactor (900 °C–1050 °C) to enhance reaction 3 and increase the carbon content of reduced iron [13].

Rostrup-Nielsen and Christiansen [14] propose three different ways to evaluate the potential for carbon deposition of a given gas mixture in syngas production. The first one is the Principle of the Equilibrated Gas, in which the final state of thermodynamic equilibrium is calculated, and carbon activity is evaluated at such conditions. One single value for carbon activity is obtained which makes it easy to compare different conditions.

The other two approaches are not at equilibrium conditions. The more conservative method is the Principle of the Actual Gas, in which the three carbon-forming reactions are considered separately. Carbon activity is calculated for each reaction, resulting in three different values. When $a_C \geq 1$ for at least one reaction, carbon deposition may be expected. This is the easiest method, because no complicated calculations are required. However, the obtained carbon activities for the three reactions may be misleading since they may differ much from one to another.

The third way is based on the steady-state carbon activity, in which the possible formation of carbon will be the result of the rates of carbon deposition for all three reactions. This is the most complete method, since it encompass all aspects of carbon deposition, both reaction thermodynamics and kinetics. However, calculation of the rate of carbon deposition for each reaction prior to tests is usually complicated.

Equilibrium diagrams with O/C and H/C ratios being the values for the two axes are presented in the literature [14], and some authors have also proposed ternary diagrams with C, H, and O molar fractions on the three axes.

The evaluation of conditions for CVD diamond growth was performed using a C–H–O ternary graph by Wan et al. [15] and Bachman, Leers, and Lydtin [16]. Wan et al. [15] proposed a theoretic evaluation considering temperature and pressure. They performed a thermodynamic assessment on a system composed of carbon in the form of graphite and diamond. Hydrogen, and oxygen, both in the gas phase (H_2 and O_2) and atomic form (H and O) were also considered. Diamond growth domains were determined on the C–H–O graph at different pressures, temperatures, and oxygen contents. Bachman, Leers, and Lydtin [16] plotted many experimental gas compositions on a C–H–O chart in which they were able to set boundaries for the diamond growth domain. However, they did not consider the temperature and pressure in performed experiments. The points obtained at different conditions were plotted on the same chart.

Li et al. [17] developed a non-stoichiometric equilibrium model based on free energy minimization for coal gasification. C, O, H, N, and S were the elements considered in the model in the form of 42 different gas and solid species. The authors calculated system compositions in which 99% of solid carbon is gasified at different temperatures and pressures, and 1% remains in solid-state. Muramoto et al. [18] did a calculation for carbon deposition on solid oxide fuel cells (SOFC) considering H_2, H_2O, CO, CO_2, CH_4 as gaseous species and solid carbon. Calculations were performed both analytically and using thermodynamic simulators (HSC® [19] and FactSage® [20]). The final solid carbon amount in the system was set to be 1 ppmw of its original content. In both studies, the presence of carbon in final states, even in low amounts, shows that gas compositions must be in equilibrium with solid carbon of unitary activity.

Takeguchi et al. [21] also presented C–H–O charts for analyzing thermodynamic equilibrium conditions in gas mixtures. They considered the same chemical species as Muramoto et al. [18]. However, they did not specify how the calculation was performed. The final charts showed the boundaries for the carbon deposition region at different temperatures.

Jaworski and Pianko-Oprych [22] evaluated carbon deposition in the reforming of hydrocarbons. Five different solid carbon allotropes were considered: graphite, diamond, amorphous, multi-walled carbon nanotubes, and single-walled nanotubes in bundles. The calculation was performed in the HSC software. The results showed that the domain for carbon deposition only in the form of graphite is smaller than the domain calculated when all allotropes were considered in the calculation.

Lal [23] calculated C–H–O graphs with carbon iso-activity lines at different temperatures and pressures, assessing the effect of gas compositions on the growth of carbon nanotubes. The author programmed the MathCad® software to solve a system of non-linear equations in which the solid carbon activity, the oxygen, and hydrogen partial pressure may be predefined, as well as temperature and pressure. The program calculates the gas compositions in equilibrium in such conditions.

Some of the diagrams from previous studys were about diamond growth [15,16], which is a different application of what is proposed in the present work. Most of previous

diagrams did not considered carbon activity valuers different than one [15–18,21,22] and that is of importance for quantifying the potential for carbon deposition. Lal [23] is the only author that presented diagrams with lines of different carbon activities, however calculations required the use of a solver. Others works [18,22] used simulation softwares, requiring those tools for replicating the results and making new diagrams for new set of conditions.

In the present work, a thermodynamic analysis of carbon-forming reactions was performed. The result is a graphic display of the equilibrium carbon activity for different gas compositions in various temperatures and pressures. All the steps for calculating gas compositions in equilibrium with defined carbon activities are shown. The thermodynamic model was solved analytically, which allows the use of this method for constructions of other diagrams based on conditions of interest without the need of any simulation software or solver. The proposed ternary diagram is a straightforward way to determine the carbon activity based on the Principle of the Equilibrated Gas. Moreover, the diagram is used to analyze possibility of carbon deposition in conditions related to the direct reduction of iron ore and reforming of methane, methanol, and ethanol.

2. Thermodynamic model of carbon deposition reactions

The chemical reactions 1 and 2 are exothermic and favored at lower temperatures (typically < 860 °C). Reaction 3 is endothermic and favored at higher temperatures (usually> 1000 °C) [9].

The potential for carbon deposition given by carbon activity can be calculated for each of these reactions by Eqs. (4)–(6). The partial pressures of the gases are identified as p_i. The values of the Gibbs Free Energy (ΔG^0) were obtained at FactSage 7.1 thermodynamic package, and equilibrium constants (K_1, K_2, and K_3) were calculated from such data.

$$a_{C_1} = K_1 \cdot \frac{p_{CO} \cdot p_{H_2}}{p_{H_2O}} \tag{4}$$

$$a_{C_2} = K_2 \cdot \frac{(p_{CO})^2}{p_{CO_2}} \tag{5}$$

$$a_{C_3} = K_3 \cdot \frac{p_{CH_4}}{(p_{H_2})^2} \tag{6}$$

Fig. 1 shows the carbon activity for typical syngas produced by steam methane reforming (SMR) for each of the carbon forming reactions (Eqs. (1)–(3)). The pressure is 20 bar, and gas composition in volume percentages is shown in Table 1. The reactor exit temperature for SMR is around 850 °C, and carbon activity will be lower than one for all reactions. Temperatures lower than 800 °C could result in carbon deposition since carbon activity will be higher than one for reactions 1 and 2. Reactions were considered separately as proposed by the Principle of the Actual Gas [14].

Reactions 1–3 must be jointly considered to perform the equilibrium analysis for the whole gas mixture as in the Principle of the Equilibrated Gas [14]. Therefore, there is a system of equations composed by Eqs. (4)–(6) and Eq. (7) that represents the total pressure, p_{total}, obtained by the sum of the partial pressure of each gas.

$$p_{CO} + p_{CH_4} + p_{CO_2} + p_{H_2} + p_{H_2O} = p_{total} \tag{7}$$

Since the system has four equations and five unknowns, which are the gases' partial pressures, more than one gas composition will be equilibrated with a given carbon activity at specific temperature and pressure (p_{total}).

Eq. (8) is obtained by applying Eqs. (4)–(6) to (7).

$$p_{CO} + p_{CO}{}^2\frac{K_2}{a_c} + \frac{p_{H_2}{}^2}{K_3/a_C} + p_{H_2} + p_{H_2}p_{CO}\frac{K_1}{a_C} = p_{total} \tag{8}$$

Rearranging Eq. (8) results in a quadratic equation (Eq. (9)) in terms of pH_2, with γ_1 being the quadratic coefficient, γ_2 being the linear coefficient, and γ_3 the constant term.

$$\gamma_1 \cdot p_{H_2}{}^2 + \gamma_2 \cdot p_{H_2} + \gamma_3 = 0 \tag{9}$$

where, $\gamma_1 = \frac{1}{K_3/a_C}$; $\gamma_2 = \left(1 + p_{CO}\frac{K_1}{a_C}\right)$; $\gamma_3 = \left(p_{CO} + p_{CO}{}^2\frac{K_2}{a_C} - p_{total}\right)$

For obtaining real roots for Eq. (9), the discriminant must be positive ($\Delta_{eq.\ 09}$), as shown in Eq. (10). From this condition, two boundaries for pCO are obtained. Eq. (11) shows such boundaries in the case for $\gamma_4 > 0$. When $\gamma_4 < 0$, the obtained values for pCO are not real numbers and do not have any physical meaning.

$$\Delta_{eq.\ 09} > 0 \rightarrow \gamma_2{}^2 - 4 \cdot \gamma_1 \cdot \gamma_3 > 0 \rightarrow \gamma_4 \cdot p_{CO}{}^2 + \gamma_5 \cdot p_{CO} + \gamma_6 > 0 \tag{10}$$

where, $\gamma_4 = \left(-4\frac{K_2}{a_C} + \frac{K_3}{a_C}\left(\frac{K_1}{a_C}\right)^2\right)$; $\gamma_5 = \left(2\frac{K_1}{a_C}\frac{K_3}{a_C} - 4\right)$; $\gamma_6 = \left(\frac{K_3}{a_C} + 4p_{total}\right)$

$$\frac{-\gamma_5 - \sqrt{\gamma_5{}^2 - 4\gamma_4\gamma_6}}{2\gamma_4} < p_{CO} < \frac{-\gamma_5 + \sqrt{\gamma_5{}^2 - 4\gamma_4\gamma_6}}{2\gamma_4} \tag{11}$$

The solution for Eq. (9) is shown in Eq. (12).

$$p_{H_2} = \frac{-\gamma_2 \pm \sqrt{\gamma_2{}^2 - 4\gamma_1\gamma_3}}{2\gamma_1} \tag{12}$$

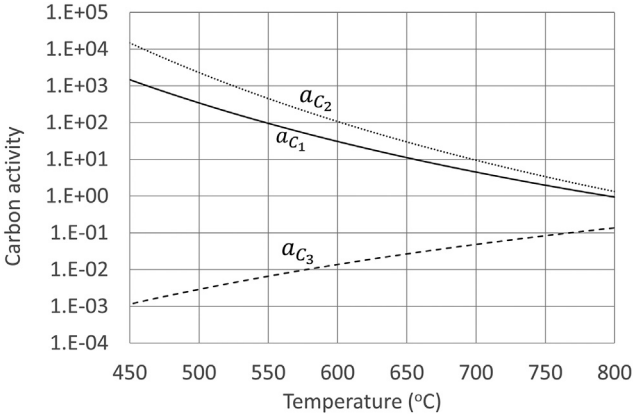

Fig. 1 – Carbon activities calculated for syngas produced by SRM at different temperatures. Total pressure at 20 atm [9].

Table 1 – Gas compositions in molar percentage of direct reduction processes and steam reforming of methane (SMR), methanol and ethanol.

	CO	H_2	CO_2	H_2O	CH_4	CH_3OH	C_2H_5OH	Ref.
Energiron ZR	15.0	60.0	0.0	5.0	20.0	0.0	0.0	[24]
Midrex	34.7	53.0	2.5	5.2	4.7	0.0	0.0	[25]
Methanol reforming	0.0	0.0	0.0	60.0	0.0	40.0	0.0	[26]
Ethanol reforming	0.0	0.0	0.0	75.0	0.0	0.0	25.0	[27]
SMR Syngas	13.6	56.5	4.1	21.8	4.1	0.0	0.0	[9]

Since $\gamma_1 > 0$ and $\gamma_2 > 0$, there is only one positive solution that is presented in Eq. (13). Additionally, the inequality of Eq. (14) must be met for pH_2 to be positive, and two more boundary conditions for pCO arise from that. These are shown in Eq. (15). Applying the values of K_1, K_2, and K_3 in the temperature range of this work, as well as with carbon activities between 10^{-4} and 10^{2}, the only condition that limited pCO is that displayed in Eq. (16) - which is the upper level of Eq. (15). The other boundaries for pCO are met numerically in all calculations, but they are not useful in representing real conditions (e.g., the upper bound of Eq. (11) often resulted in $pCO > p_{total}$).

$$p_{H2} = \frac{-\gamma_2 + \sqrt{\gamma_2{}^2 - 4\gamma_1\gamma_3}}{2\gamma_1} \tag{13}$$

$$-\gamma_2 + \sqrt{\gamma_2{}^2 - 4\gamma_1\gamma_3} > 0 \tag{14}$$

$$\frac{-2\frac{K_1}{a_C} + \frac{\gamma_5}{K_3} - \sqrt{4\left(\frac{K_1}{a_C}\right)^2 \cdot \frac{\gamma_6}{K_3} - 4\frac{K_1}{a_C}\frac{\gamma_5}{K_3} - 4\frac{\gamma_4}{K_3}\frac{\gamma_6}{K_3} + 4\frac{\gamma_4}{K_3} + \left(\frac{\gamma_5}{K_3}\right)^2}}{2\left(\left(\frac{K_1}{a_C}\right)^2 - \frac{\gamma_4}{K_3}\right)} < p_{CO} < \frac{-2\frac{K_1}{a_C} + \frac{\gamma_5}{K_3} + \sqrt{4\left(\frac{K_1}{a_C}\right)^2 \cdot \frac{\gamma_6}{K_3} - 4\frac{K_1}{a_C}\frac{\gamma_5}{K_3} - 4\frac{\gamma_4}{K_3}\frac{\gamma_6}{K_3} + 4\frac{\gamma_4}{K_3} + \left(\frac{\gamma_5}{K_3}\right)^2}}{2\left(\left(\frac{K_1}{a_C}\right)^2 - \frac{\gamma_4}{K_3}\right)} \tag{15}$$

$$p_{CO\,max} = \frac{-2\frac{K_1}{a_C} + \frac{\gamma_5}{K_3} + \sqrt{4\left(\frac{K_1}{a_C}\right)^2 \cdot \frac{\gamma_6}{K_3} - 4\frac{K_1}{a_C}\frac{\gamma_5}{K_3} - 4\frac{\gamma_4}{K_3}\frac{\gamma_6}{K_3} + 4\frac{\gamma_4}{K_3} + \left(\frac{\gamma_5}{K_3}\right)^2}}{2\left(\left(\frac{K_1}{a_C}\right)^2 - \frac{\gamma_4}{K_3}\right)} \tag{16}$$

Lastly, to calculate the lines in the ternary diagram based on the equations shown above, the following procedure was used:

- Equilibrium constants (K_1, K_2 and K_3) are calculated from defined temperature.
- Carbon activity and total pressure (p_{total}) are set.
- pCO_{max} is calculated from Eq. (16).
- pH_2 is calculated using Eq. (13) for different gas compositions by varying pCO from zero to pCO_{max}.
- pCO_2, pCH_4, and pH_2O are computed using Eqs. (4)–(6) for each combination of pCO and pH_2.

Equilibrium results of such gas mixtures are usually presented in graphs that O/C and H/C ratios are the values for the two axes [14]. Nevertheless, the H/O ratio is also important. To present the three molar fractions O, C, and H_2 on the axes of a graph, equilibrium carbon activities were plotted in a ternary diagram. Gas compositions are shown as molar fractions of C, O, and H_2, calculated according to Eqs. (17)–(23).

$$n_C = y_{CO} + y_{CO_2} + y_{CH_4} \tag{17}$$

$$n_{H_2} = y_{H_2} + y_{H_2O} + 2\,y_{CH_4} \tag{18}$$

$$n_O = y_{CO} + 2\,y_{CO_2} + y_{H_2O} \tag{19}$$

where y_i is the molar fraction of gas i.

$$n_T = n_C + n_O + n_{H_2} \tag{20}$$

$$C = \frac{n_C}{n_T} \tag{21}$$

$$O = \frac{n_O}{n_T} \tag{22}$$

$$H_2 = \frac{n_{H_2}}{n_T} \tag{23}$$

Ternary diagrams calculated at different temperatures, pressures and carbon activities are presented below.

3. Results and discussion

The C–O–H_2 diagram of iso-activity lines of unitary carbon activity at different temperatures and total pressure of 1 atm is shown in Fig. 2. The lines are the set of gas compositions in thermodynamic equilibrium with solid carbon. The region above each line represents gas compositions with potential for carbon deposition at each temperature.

At 200 °C and 400 °C, the lines intersect the OC axis close to the CO_2 point, which means that small amounts of CO would be enough for obtaining carbon activities equal or higher than one. And in such cases, there is thermodynamic potential for carburization due to disproportionation of CO (reaction 2). On the other hand, these lines intersect the CH_2 axis close to the CH_4 point, showing that carbon deposition due to methane decomposition is not expected at such low temperatures. It is also observed that the curves bend towards the H_2O point, indicating that unitary equilibrium

carbon activity for reaction 1 is reached even with a high content of H_2O.

As temperature increases, CO becomes more stable, and methane begins to be the main carburizing agent. Therefore, iso-activities lines of unitary carbon activity tend to approximate to the CO point and to distance from the CH_4 point. Accordingly, the curvilinear aspect of low temperature curves disappears, as equilibrium of reaction 1, with unitary carbon activity displaces in the direction of the reagents (CO and H_2). At temperatures equal and higher than 900 °C, gas compositions in equilibrium with solid carbon, lay approximately in the line connecting CO and H_2 points. The presence of H_2O in the gas mixture would reduce the equilibrium carbon activity and the presence of methane would cause the opposite effect.

At intermediate temperatures, between 400 °C and 900 °C, both CO and CH_4 may act as carburizing agents according to reactions 1, 2 and 3.

Figs. 3 and 4 presents a similar C–O–H_2 diagram for total pressures of 7 atm and 20 atm, respectively. Increase in total pressure displaces the equilibrium of reactions 1 and 2 towards the products favoring carburization due to CO disproportionation and CO reduction by H_2. However, the equilibrium of reaction 3 is displaced towards methane, making it a weaker carburizing agent. The changes caused by pressure increase are observed in the iso-activity lines, as the ends that intersect the OC axis divert from the CO point and get closer to the CO_2 point, and the opposite ends approximate the CH_4 point. Additionally, the lines of 700 °C, 800 °C and 900 °C become curved as pressure increases, showing that carbon deposition may be expected from gas mixtures containing higher amounts of H_2O.

Fig. 5 shows the changes in iso-activities for different pressures at temperatures of 400 °C, 700 °C and 1100 °C. The change in pressure has a more significant impact on the line for 700 °C, since all three carbon forming reactions are relevant in that temperature. For 1100 °C, carburization is expected to occur mainly due to methane decomposition (reaction 3), and more notable changes were observed in the end that intersects the CH_2 axis. For 400 °C, lines are remarkably close to CO_2 point and could not move further in that direction as pressure increases, and some changes are also observed in the CH_2 axis, as lines divert from the CH_4 point.

All the observed changes in iso-activity lines for unitary carbon activity at different temperatures and pressures are result of the equilibrium of the three carbon forming reactions considered jointly. Therefore, diagrams presented in Figs. 2–5 are helpful in evaluating the effect of process variables in the potential for carbon deposition.

To quantify the potential for carbon deposition of a given gas mixture, the activity of solid carbon in equilibrium with such gas mixture has to be calculated. Iso-activity lines for different carbon activities at total pressure of 1 atm and temperatures of 400 °C and 1100 °C are showed in Fig. 6.

At 400 °C, gas mixtures with carbon activities equal to and lower than 10^{-3} lies approximately in the line connecting the CO_2, H_2O and H_2 points, which shows that small amounts of CO or CH_4 would cause an increase in carbon activity. On the other hand, gas mixtures with carbon activities of 50 and 100 lie approximately in the line connecting CO_2 and CH_4. In such conditions, the p_{COmax} obtained from Eq. (16) for carbon activity of 100 was 8.2×10^{-2} atm. Higher CO contents would result in even higher equilibrium carbon activities.

At 1100 °C, it is difficult to distinguish gas compositions in equilibrium with carbon activities in the range of 10^{-1} to 10, as

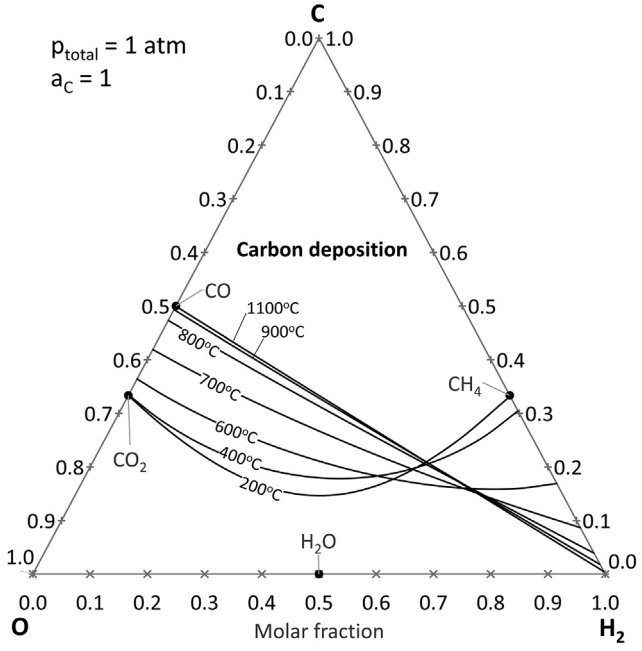

Fig. 2 – C–O–H_2 diagram showing iso-activities ($a_C = 1$) lines for different temperatures and total pressure of 1 atm.

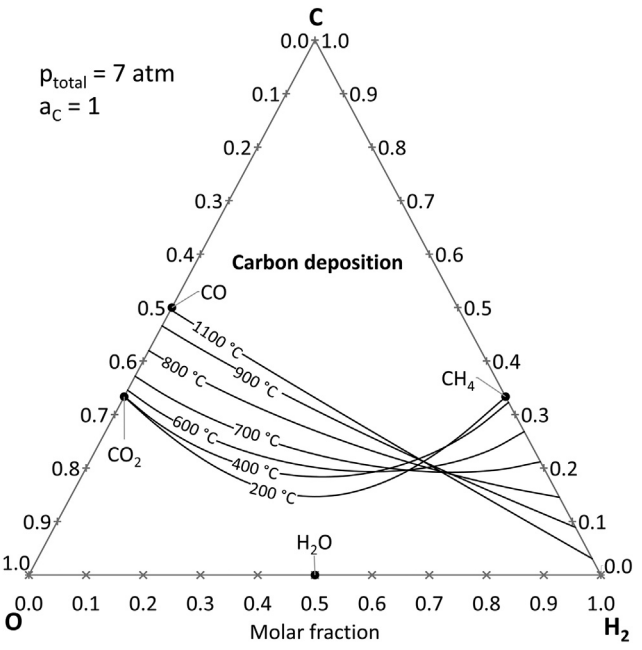

Fig. 3 – C–O–H_2 diagram showing iso-activities ($a_C = 1$) lines for different temperatures and total pressure of 7 atm.

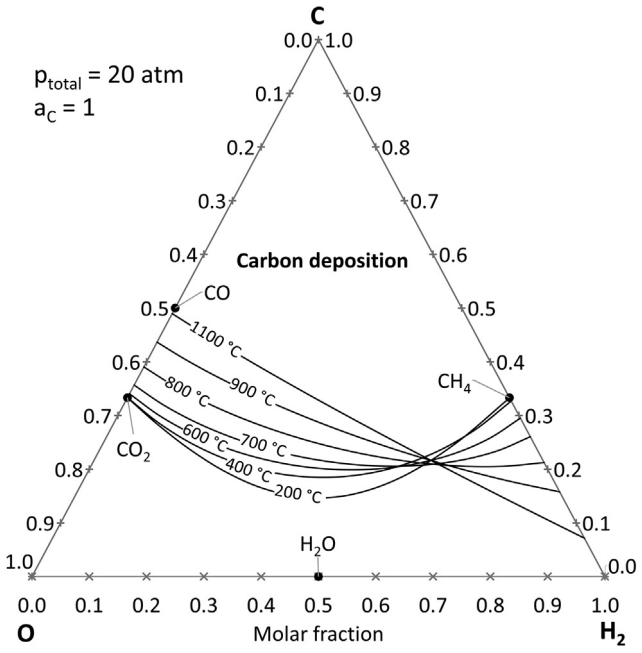

Fig. 4 – C–O–H_2 diagram showing iso-activities ($a_C = 1$) lines for different temperatures and total pressure of 20 atm.

lines are close to each other. This means that small changes in gas compositions around those lines will have major impact in the carbon activity in equilibrium with such gas composition. Lines for carbon activities lower than 10^{-1} are closer to CO_2 and H_2O points and lines for 50 and 100 shift towards CH_4.

Fig. 7 presents iso-activity lines for different carbon activities and different total pressures at 400 °C and 1100 °C. At 400 °C, change in total pressure from 1 to 20 atm had small effect on iso-activity lines for carbon activities of 1 up to 100. Therefore, carbon activities in equilibrium with gas mixtures in such regions of the C–O–H_2 diagram would not be significantly altered as pressure is increased. For carbon activities of 10^{-2}, the change in total pressure has no apparent effect on the section connecting CO_2 to H_2O, but lines shifted towards methane as pressure increases.

At 1100 °C, increasing total pressure has a different effect whether carbon activity is higher or lower than one. Lines for carbon activities of one and higher are straight starting close to the CO point for all considered pressures. As total pressure increases, the other end moves in the direction of the CH_4 point, showing that higher contents of methane and lower contents of H_2O, H_2 and CO_2 are required for maintaining the same carbon activity. Lines for carbon activities lower than one move away from CH_4 and CO as pressure increases, meaning that lower amounts of such gases and higher amounts of H_2O and CO_2 are necessary to maintain carbon activity constant.

Diagrams of Fig. 2 through 5 allow evaluation whether a gas mixture of interest has or has not potential to cause carbon deposition. Figs. 6 and 7 permit a deeper and more precise analysis, as quantitative values for carbon activities are taken from such diagrams. These values are direct measures on the equilibrium potential for carbon deposition.

Activities lower than one are also of interest, since carbon can not only deposit onto but also dissolve in some metallic compounds. Moreover, it is possible to determine the equilibrium carbon content in the solid metal based on the carbon activity in the gas.

3.1. *Application of the ternary C–O–H_2 diagram in direct reduction of iron and in reforming of hydrocarbons*

The C–O–H_2 ternary diagram will be applied to analyze gas compositions of direct reduction of iron and reforming of hydrocarbons. Gas compositions of such processes are listed in Table 1. Nitrogen and other hydrocarbons were not considered for gas compositions of Energiron ZR (24) and Midrex (25) process gases. SMR syngas is the outlet gas composition with steam-to-carbon (S/C) ratio of 2.5. Methanol and ethanol reforming are the inlet compositions with S/C of 1.5, which is

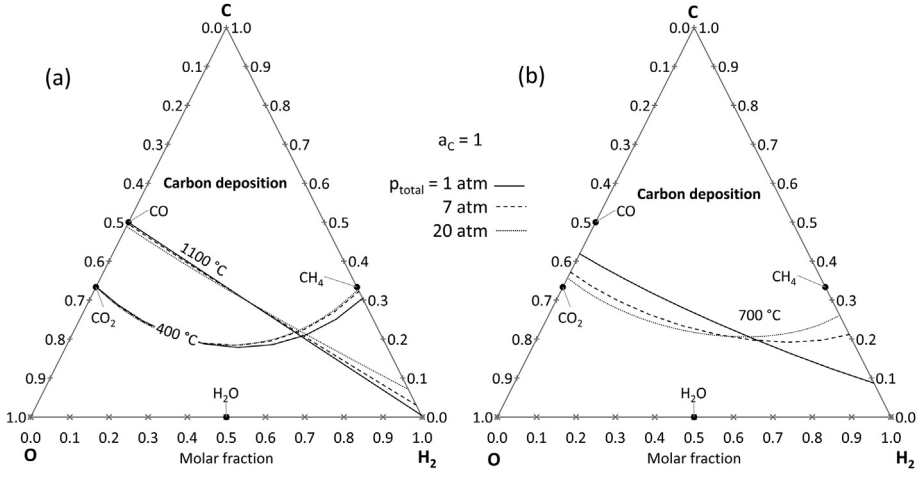

Fig. 5 – C–O–H_2 diagram showing iso-activities ($a_C = 1$) lines for different temperatures pressures.

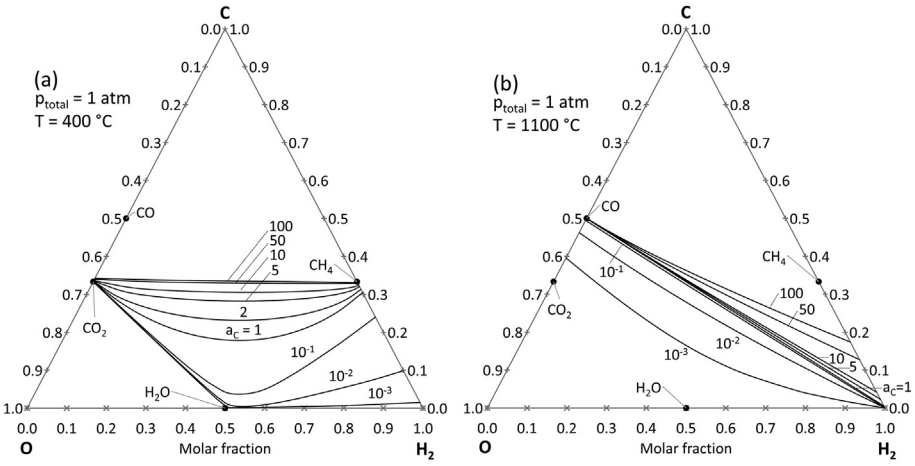

Fig. 6 – Lines for different carbon activities (a_C) at 400 °C and 1100 °C and total pressure of 1 atm.

the usual S/C for methanol reforming [26]. In the case of ethanol reforming, other S/C are also used depending of the process (27), and the value of 1.5 was chosen for this work.

3.1.1. *Application of the ternary C–O–H_2 diagram in the direct reduction of iron*

The composition of the bustle gas of Midrex (25) and Energiron ZR [24] direct reduction processes are presented in Fig. 8. Midrex and Energiron ZR compositions show different carbon activities at the usual operating conditions of temperature and pressure of each process. The Midrex process operates close to atmospheric pressure, while Energiron ZR operates at 6–8 atm at the injection point of the reducing gas.

Carbon activity in equilibrium with Midrex gas at 1 atm (Fig. 2) is 0.15 at 1000 °C. Industrially, the reducing gas is injected at the bottom of the reduction zone at temperatures above 950 °C. Carbon may be incorporated in iron in solid solution. At 1000 °C, iron is in the form of austenite and the equilibrium content of dissolved carbon with activity of 0.15 is 0.35 wt %. This value was calculated in FactSage™ 7.1 using FStel database. This is an example in which carbon activities lower than one are of interest to understand the equilibrium condition of the industrial system.

The diagram of Fig. 2 shows that carbon activity of the MIDREX bustle gas would be higher than one at lower temperatures, more specifically, below 900 °C. This means lower bustle temperature would favor carburization. However, the rate of reduction reactions would decrease and negatively impact process productivity. To overcome that problem and increase carbon content of reduced iron pellets, natural gas is injected just below the reduction zone where solids are at high temperature (>900 °C). This favors reaction 3. The discharged material contains about 2,5 wt.% of carbon (12).

Energiron ZR gas is in equilibrium with carbon activity of 8.5 at 1100 °C and 7 atm. The gas is injected in the reactor at the bottom of the reduction zone at temperatures above 1050 °C. Carbon deposition is expected as a result of the contact of reducing gases and solid reduced iron pellets. The discharged material of Energiron ZR may contain up to 4,5 wt.% of carbon, which is higher than the value obtained with the Midrex process.

Based on the proposed diagram, it is simple to compare the gas compositions of the two processes (Midrex and Energiron ZR) and explain the difference of carbon content on the product by observing the equilibrium carbon activity of the reducing gases.

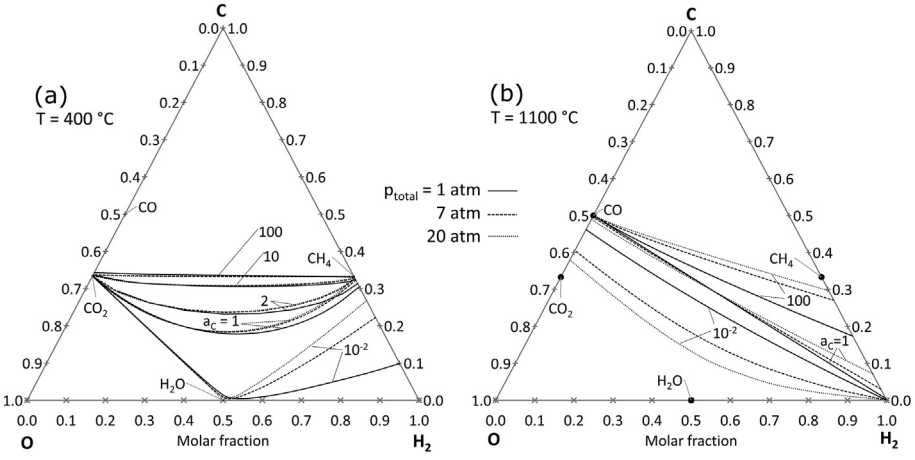

Fig. 7 – Lines for different carbon activities (a_C) at 400 °C and 1100 °C and different total pressures.

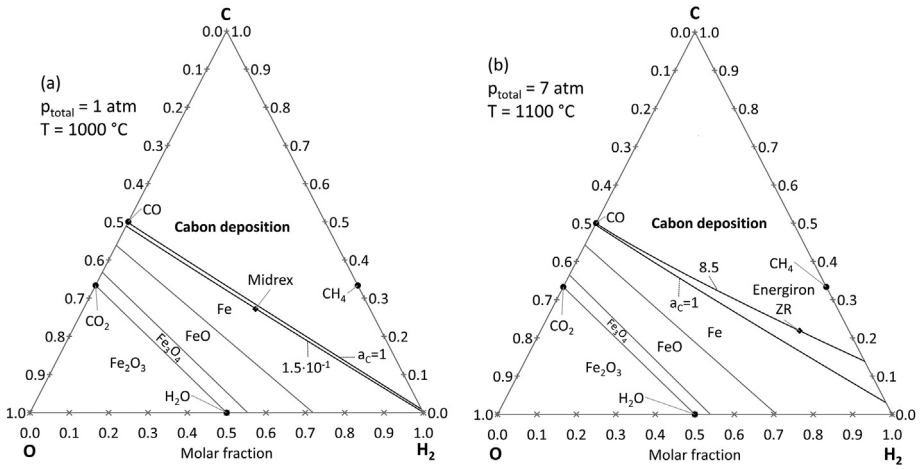

Fig. 8 – Application of the ternary C–O–H_2 diagram for direct reduction processes showing carbon activity in equilibrium with bustle gas of (a) the Midrex process and (b) the Energiron ZR process.

It is also possible to calculate gas mixtures composed of H_2, CO, CO_2 and H_2O that are in equilibrium with iron oxides and metallic iron. The procedure is analogous to what was performed to determine gas compositions in equilibrium with different carbon activity. The curves for reduction reactions are also presented in Fig. 8 and both Midrex and Energiron compositions are within the predominance area of metallic iron and far from the FeO/Fe transition, showing a high reducing potential. The authors of this work have used this graph to compare different gas compositions according to their equilibrium carbon activity and reducing potential for iron oxides [28]. Gas compositions were selected in order to avoid oxidation of reduced iron pellets and to vary the carburization potential.

3.1.2. *Application of the ternary C–O–H_2 diagram for reforming of hydrocarbons*

Lately, steam reforming of methane, methanol and ethanol are gaining attention for the production of hydrogen.

A typical syngas composition produced by SMR (9) at 850 °C is presented in Fig. 9a. At 850 °C, equilibrium carbon activity is 0.35. Methanol reforming gas is shown in Fig. 9b at 240 °C and 2 atm that are usual industrial conditions [26]. In such conditions, carbon activity is equal to 0.73. Therefore, carbon deposition is not thermodynamically favored for SMR and methanol reforming in such conditions. The carbon activity for methanol reforming is higher, and in the presence of iron from steel reactor walls or iron-based catalysts, more carbon is expected to dissolve in solid iron.

Ethanol reforming is still under development, and different conditions are found in the literature. Hence, a diagram with temperatures of 240 °C, 500 °C and 850 °C and pressures of 2 atm and 20 atm is presented in Fig. 10. This diagram shows that ethanol reforming gas is on the line of carbon activity of one at 240 °C. At this temperature, the change of pressure from 2 atm to 20 atm has little influence on the equilibrium carbon activity line. At 500 °C and 850 °C, carbon activity is lower than one for both pressure levels and carbon deposition is not expected in equilibrium conditions.

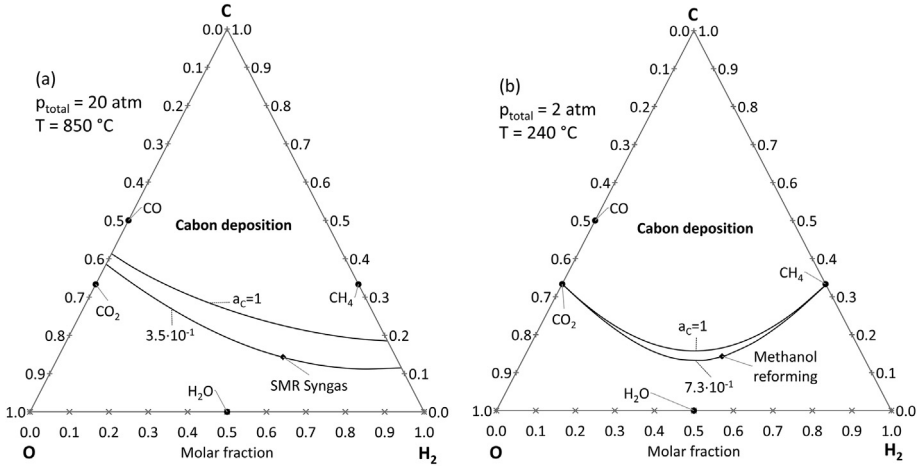

Fig. 9 – Application of the ternary C–O–H_2 diagram for (a) steam methane reforming (SMR) at 850 °C and 20 atm and for (b) methanol reforming at 240 °C and 2 atm.

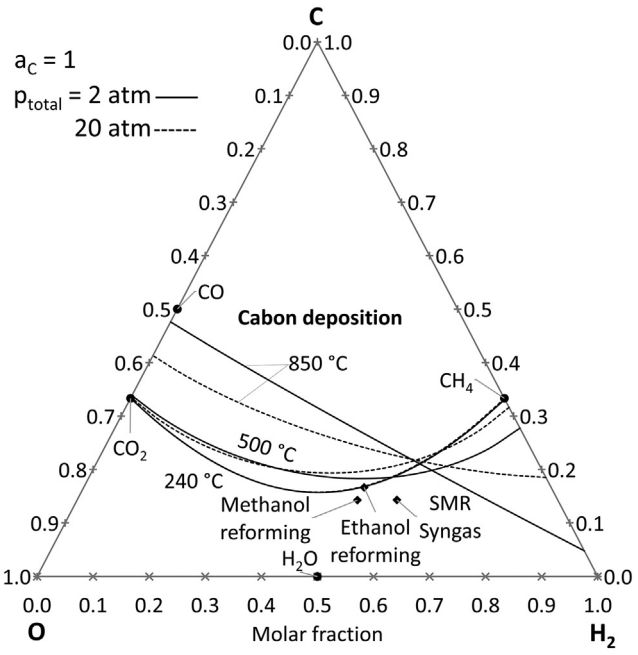

Fig. 10 – Application of the ternary C–O–H_2 diagram for steam methane (SMR), methanol and ethanol reforming at different temperatures and pressures.

Fig. 1 showed that, at temperatures lower than 800 °C, the SRM syngas could cause carbon deposition due to reactions 1 and 2. However, this carbon could be consumed by the reverse of reaction 3 since carbon activity is lower than one for this reaction. The graph in Fig. 10 takes all of this into consideration and gives the overall equilibrium condition. Even at low temperatures as 240 °C, SMR syngas is under the lines for carbon activity of one and carbon activity is not expected in equilibrium conditions. The same is valid for methanol reforming.

The observed difference on the ethanol reforming gas is related to the higher amount of carbon in the molecule in comparison to the methanol molecule. So, ethanol reforming gas has higher C/O ratio than the methanol reforming gas, even though the S/C is the same for both.

Methanol and ethanol were not considered in the thermodynamic model presented in equations [7–16]. However, reaction mechanism of carbon deposition for both components occurs through decomposition to methane or formation of CO or CO_2 [27,29,30]. From that, carbon is then adsorbed on the catalyst surface. This means that the proposed thermodynamic model can be of use for methanol and ethanol reforming.

It is very common in the study of reforming of hydrocarbons, the computation of the amount of deposited carbon after the study of a determined catalyst. It is suggested that a comparison between different catalysts should be performed with equal or similar carbon activity in equilibrium with the tested gas mixture. Hence, catalyst tendence for carbon deposition will not be erroneously affected by a different (higher or lower) potential for carbon deposition, i.e., higher carbon activity in equilibrium with the used gas mixture.

4. Summary and conclusions

An analytical model for calculating carbon activity with gas mixtures containing CH_4, H_2, H_2O, CO and CO_2 was proposed. The results were composed of iso-activity lines for carbon activity in different temperatures and pressures plotted in a ternary C–O–H_2 diagram. The proposed diagram is a simple way of displaying equilibrium carbon activities at different conditions and gas compositions. The customization of such diagram may be useful in comparing different process conditions, selecting gas mixtures, and evaluating carburization potential in industrial processes.

Using the proposed diagram, it was possible to verify that carbon activity in equilibrium with the direct reduction process gas of Midrex process is of 0.15 and of Energiron ZR process is of 8.5, explaining the higher carbon content in the reduced iron for the latter.

In the case of reforming of hydrocarbons, equilibrium carbon activity in usual industrial conditions for steam reforming of methane and methanol are 0.35 and 0.73, respectively. This means, that carbon deposition is not expected in equilibrium conditions. For ethanol reforming, carbon deposition is expected at 240 °C and this would be prevented at temperatures equal or higher of 500 °C and pressures between 2 atm and 20 atm.

The proposed diagram could be useful in many chemical, catalytic, and metallurgical processes for study or prevention of carbon formation.

Declaration of Competing Interest

The authors declare that they have no known competing financial interests or personal relationships that could have appeared to influence the work reported in this paper.

Acknowledgements

The authors would like to thank the Research Council of Norway (GASFERROSIL project - grant number: 224950/E30) and FIPT (The Foundation for the Support of the Institute for Technological Research) for financially supporting this project. The authors also thank André Nunis da Silva for assitining in the revision of final manuscript.

REFERENCES

[1] Trimm DL. Coke formation and minimisation during steam reforming reactions. Catal Today 1997;37:233–8.
[2] Trimm DL. The formation and removal of coke from nickel catalyst. Catal Rev Sci Eng 1977;16(2):155–89.
[3] Grabke HJ, Krajak R, Nava Paz JC. On the mechanism of catastrophic carburization: 'metal dusting. Corrosion Sci 1993;35(5):1141–50.
[4] Grabke HJ. Thermodynamics, mechanisms and kinetics of metal dusting. Mater Corros 1998 May;49(5):303–8.

[5] Grabke HJ, Moller-Lorenz EM, Schneider A. Carburlzation and metal dusting on lron. ISIJ Int 2001;41:S1–8.
[6] Grabke HJ. Metal dusting. Mater Corros 2003 Oct;54(10):736–46.
[7] Young DJ, Zhang J, Geers C, Schütze M. Recent advances in understanding metal dusting: a review. Mater Corros 2011 Jan 1;62(1):7–28.
[8] Young DJ, Zhang J. Carbon corrosion of alloys at high temperature. J South African Inst Min Metall 2013;113(2):149–54.
[9] Hirotani K. Metal dusting -severe problem in operation of syngas generation for GTL plant. In: Proceedings of the fifteenth international offshore and polar engineering conference [internet]. Seoul, Korea; 2005 [cited 2016 Dec 16]. Available from: https://www.onepetro.org/download/conference-paper/ISOPE-I-05-009?id=conference-paper%2FISOPE-I-05-009.
[10] Holland ML, De Bruyn HJ. Metal dusting failures in methane reforming plant. Int J Pres Ves Pip 1996;66(1–3):125–33.
[11] Grabke HJ. Evidence on the surface concentration of carbon on gamma iron from the kinetics of the carburization in CH4–H2. Metall Trans 1970;1(10):2972–5.
[12] D'Abreu JC, Otaviano MM, Kohler HM. Kinetic of dri carburization in shaft furnaces. In: 6th int congress on the science and technology of ironmaking 2012, ICSTI 2012 - including proceedings from the 42nd ironmaking and raw materials seminar, and the 13th Brazilian symp on iron ore. Rio de Janeiro; 2012. p. 2327–36.
[13] Griscom FN, Metius GE, e Kopfle JT. Ironmaking technology for the new millennium. NC: Charlotte; 2000.
[14] Rostrup-Nielsen JR, Christiansen LJ. In: Edit First, Hutchings GJ, editors. Concepts in syngas manufacture. Londres: Imperial College Press; 2011.
[15] Wan YZ, Zhang DW, Liu ZJ, Wang JT. Effects of temperature and pressure on CVD diamond growth from the C-H-O system. Appl Phys A Mater Sci Process 1998;67(2):225–31.
[16] Bachmann PK, Leers D, Lydtin H. Towards a general concept of diamond CVD. Diam Relat Mater 1991;1.
[17] Li X, Grace JR, Watkinson AP, Lim CJ, Ergüdenler A. Equilibrium modeling of gasification: a free energy minimization approach and its application to a circulating fluidized bed coal gasifier. Fuel 2001;80(2):195–207.
[18] Muramoto A, Kikuchi Y, Tachikawa Y, Lyth SM, Shiratori Y, Taniguchi S, et al. High-pressure C-H-O diagrams: fuel composition, carbon deposition, and open circuit voltage of pressurized SOFCs. Int J Hydrogen Energy 2017;42(52):30769–86.
[19] Outotec. HSC chemistry 10. 2020. Available at: https://www.outotec.com/products/digital-solutions/hsc-chemistry.
[20] Bale CW, Bélisle E, Chartrand P, Decterov SA, Eriksson G, Gheribi AE, et al. FactSage Thermochemical Software and Databases - 2010–2016. Calphad 2016;54:35–53. www.factsage.com.
[21] Takeguchi T, Kani Y, Yano T, Kikuchi R, Eguchi K, Tsujimoto K, et al. Study on steam reforming of CH4 and C2 hydrocarbons and carbon deposition on Ni-YSZ cermets. J Power Sources 2002;112(2):588–95.
[22] Jaworski Z, Pianko-Oprych P. A comparative thermodynamic study of equilibrium conditions for carbon deposition from catalytic C-H-O reformates. Energies 2018;11(5).
[23] Lal A. Effect OF gas composition and carbon activity ON the growth OF carbon nanotubes [Internet]. University of Florida; 2003. Available from: etd.fcla.edu/UF/UFE0001151/lal_a.pdf.
[24] Celada-Gonzales J, Quintero-Flores RG, Viramontes-Brown R, Flores Serrano RO. Apparatus for producing direct reduced iron with a controlled amount of carbon. US: USPTO; US 6039916A. 2000. p. 6.
[25] Parisi DR, Laborde MA. Modeling of counter current moving bed gas-solid reactor used in direct reduction of iron ore. Chem Eng J 2004;104(1–3):35–43.
[26] Iulianelli A, Ribeirinha P, Mendes A, Basile A. Methanol steam reforming for hydrogen generation via conventional and membrane reactors: a review. Renew Sustain Energy Rev 2014 Jan;29:355–68.
[27] Guerrero L, Castilla S, Cobo M. Advances in ethanol reforming for the production of hydrogen. Quim Nova 2014;37(5):850–6.
[28] Ribeiro TR, Neto JBF, Poço JGR, Takano C, Kolbeinsen L, Ringdalen E. Methane reforming catalyzed by direct reduced iron. In: Proceedings of AISTech17. Nashville. USA: AIST; 2017.
[29] Zanchet D, Santos JBO, Damyanova S, Gallo JMR, Bueno JMC. Toward understanding metal-catalyzed ethanol reforming. ACS Catal 2015 Jun 5;5(6):3841–63.
[30] Amphlett JC, Evans MJ, Jones RA, Mann RF, Weir RD. Hydrogen production by the catalytic steam reforming of methanol part 1: the thermodynamics. Can J Chem Eng 1981 Dec;59(6):720–7.